This is a preprint version of

A Robust Kalman Filter Based Approach for Indoor Robot Positionning with Multi-Path Contaminated UWB Data

Accepted at the *IEEE 2023 ICASSP conference* that will be held in Rhodes, Greece.

The final version will be soon available on my IEEE Xplore author page

A ROBUST KALMAN FILTER BASED APPROACH FOR INDOOR ROBOT POSITIONNING WITH MULTI-PATH CONTAMINATED UWB DATA

Justin Cano[1,2]*, Yi Ding*[3,2]*, Gaël Pages*[2]*, Eric Chaumette*[2] *and Jerome Le Ny*[1]

[1] EE Dept. Polytechnique Montréal/GERAD, Montréal, QC, Canada.
[2] DEOS, ISAE-Supaéro, France.
[3] Airbus SAS, France.

ABSTRACT

Ultra-Wide Band (UWB) is a widely used technology to provide real-time and accurate indoor localization to mobile robots, allowing their safe operation in the absence of a satellite-based navigation solution. However, UWB performance suffers from multi-path outliers when signals reflect on surfaces or encounter obstacles. This paper describes an approach to mitigate this issue, based on a M-Estimation Robust Kalman Filter (M-RKF) and leveraging an adaptive empirical variance model for UWB signals. The approach is validated experimentally on a ground robot.

***Index Terms*—** UWB, Robotics, Navigation, RKF.

1. INTRODUCTION

Mobile robots (MR) require at all times reliable position estimates to perform their tasks accurately. Moreover, the positioning system should be low cost, consume little energy have a sufficient high refresh rate to ensure precise trajectory tracking. The design of such systems is particularly challenging for indoor localization, where Global Navigation Satellite Systems (GNSS) such as the GPS are not available. A widely used technology that meets most of the above requirements for MR indoor navigation with decimeter-level positioning accuracy is Ultra-Wide Band (UWB) [1–3]. UWB positioning uses relative distance or angle measurements between transceivers at known locations, called *anchors*, and those to localize, called *tags* [2, Chap. 4]. Position estimates can then be computed using techniques such as Least Squares (LS) or Kalman Filters (KF), as with GNSS [4].

Here, we focus on distance measurements techniques that rely on the estimation of the Time of Flight (ToF), *i.e.*, the propagation time of a signal between transceivers [1–3]. The ToF is altered in the presence of obstacles between the transceivers (Non-Line-of-Sight (NLoS) measurements) or when reflective surfaces in the environment yield Multi-Path (MP) trajectories instead of straight-line propagation [2, Chap. 4]. The resulting *outliers* in the measurements strongly deteriorate the accuracy of UWB-based positioning [1, 5] and are well studied in Radio-Frequency based navigation [4, 6].

One way to enhance the robustness of positioning algorithms to MP outliers is to detect them and reject the measurements. Recent learning-based approaches using the Channel Impulse Response (CIR) to detect outliers yield promising enhancements on positioning precision [5, 7, 8]. However, they require collecting calibration data and use significant computational resources. Alternatively, power information extracted from the CIR has also been used to identify NLoS measurements [9].

Nonetheless, outlier rejection after classification may be unsuitable when the data is strongly contaminated by MP (which implies a high rejection rate), and other strategies using filtering techniques can be used to mitigate these outliers at a higher level [10–12]. Significant improvements are also provided by using dynamic models and other sensors such as Inertial Measurement Units (IMU) [13], but in this paper we aim to mitigate outliers with only intrinsic UWB information.

We base our mitigation strategy on the M-estimation Robust KF (M-RKF) presented in [6], tailored to mitigate the effects of heavy-tailed measurement distributions. As the M-RKF algorithm has been successfully used in previous work to mitigate MP outliers in GNSS (*e.g.*, [14]), we aim to use it for indoor navigation. A NLoS bias model for UWB is provided through neural network training and used as an input in an M-REKF update in [12]. However, to compensate for the NLoS effects, this method requires an extensive training dataset and an IMU. An alternative algorithm using both a coarse outlier detection scheme and a KF based chi-square increment has been used to track a slowly moving cart in [11]. However, this system requires adjusting four hyperparameters empirically.

Here we propose a novel, empirically calibrated adaptive variance model for UWB ToF measurements, which relies on First Path Power (FPP) measurements as input that require. Then, we apply the M-RKF framework to UWB-based localization for MP-contaminated ToF data.

The rest of the paper is organized as follows. We intro-

This work was supported by FRQNT under grant 2018-PR-253646, by NSERC under grant RGPIN-5287-2018.

duce the main assumptions, the notation and the notion of MP contamination in Section 2. Then, we detail the mitigation strategy using an M-RKF and adaptive variance model in Section 3. Finally, we validate the approach in Section 4 by implementing our algorithm on a ground robot equipped with an UWB transceiver to enhance its localization, in a challenging MP-contaminated environment.

2. MULTI-PATH CONTAMINATION

Our goal is to produce an estimate $\hat{\mathbf{p}}$ of the position $\mathbf{p} \in \mathbb{R}^n$, with $n = 2$ or 3, of a MR, using UWB-based range measurements between a tag carried by the MR and a set $\mathcal{A}$ of fixed anchors whose positions $\mathbf{p}_a \in \mathbb{R}^n$, for $a \in \mathcal{A}$, are known. A ranging measurement between the tag and anchor $a \in \mathcal{A}$ is defined as $\tilde{d}_a := c\tilde{\tau}_a$, where c is the speed-of-light and the ToF $\tilde{\tau}_a$ can be estimated using a protocol such as Two-Way Ranging (TWR), which compensates for the clock drift between the transceivers [2]. In our experiments we use the TWR protocol described in [15], which computes $\tilde{\tau}_a$ after an exchange of timestamped messages between the transceivers. In standard TWR [2, Chap. 6], a first message is emitted by the tag t at time $T_{t,1}$ (according to t's clock) and received at time $R_{a,1}$ (according to a's clock) by the anchor. Then, the response is initiated by a at $T_{a,2}$ and received by t at $R_{t,2}$. Finally, the ToF can be computed as $\tilde{\tau}_a = [(R_{t,2} - T_{t,1}) - (T_{a,2} - R_{a,1})]/2$,

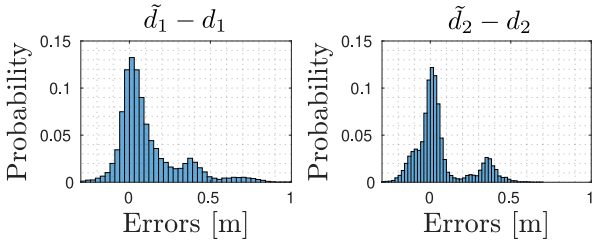

Fig. 1: Measurement error histograms with MP contamination.

Even with a perfect clock drift compensation, the actual distance $d_a := \|\mathbf{p} - \mathbf{p}_a\|$ differs from the measured $\tilde{d}_a$, which implicitly assumes straight line propagation between the transceivers. Diffraction of the signal around obstacles or reflections on surfaces such as ground or walls, i.e., MP, produce longer ToF measurements than for a direct path. As a result, the range measurement distribution becomes biased and heavy-tailed, while standard navigation filters such as the Extended K (EKF) assume measurements $\tilde{d}_a$ that are centered and possibly Gaussian [2,4]. This motivates developing better filtering methods to take MP-contamination into account.

As an illustration, we plot two histograms of UWB ranging errors $\tilde{d}_a - d_a$ on Fig. 1, based on 75000 data points. The measurements $\tilde{d}_a$ were obtained by a tag carried by a mobile robot shown in Fig. 2, while d_a was provided by a

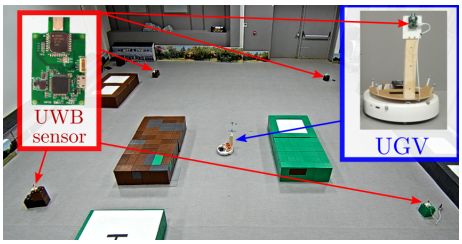

Fig. 2: Setup used for the experiments, with ground robot (UGV), UWB anchors and obstacles.

motion capture system (MCS) with negligible error. One can notice that the empirical distributions are indeed heavy-tailed, which is a result of MP effects due to ground reflection. Note that a popular modeling of the MP effect, the ϵ-contamination model, uses bimodal Gaussian distributions [6, 7.4.1].

3. MITIGATION ALGORITHM

Here, we present a method to mitigate the effects of MP contamination on positioning. First, we propose a variance model based on received power to penalize attenuated signals. Then, we present the M-RKF used to filter MP at higher level.

3.1. FPP-based Adaptive Variance Model

Previous studies [2, 9] have shown that MP contaminated signals are more attenuated than direct signals, *i.e.*, are associated with lower Reception Power (RxP). Hence, we first develop an empirical variance model, which will then be used to penalize measurements with low RxP, a standard approach in navigation [4, 14]. Moreover, the quality of the estimated reception timestamp improves with the RxP, since the detection is performed by a maximum likelihood estimator whose variance depends on the signal to noise ratio [2]. Our implementation relies on the FPP indicator extracted from the CIR of the Quorvo's DW1000 modules [16]. For each transceiver $\tau \in \{t, a\}, a \in \mathcal{A}$, the estimated reception time $\hat{R}_{\tau,i}$ is extracted from the CIR using a leading edge detection algorithm [2]. This method uses three characteristic samples of the CIR $[s_{1,i}, s_{2,i}, s_{3,i}] \in \mathbb{C}^3$, that define the received FPP by τ for the message i

$$\mathcal{P}(\hat{R}_{\tau,i}) := 10 \log \left((|s_{1,i}|^2 + |s_{2,i}|^2 + |s_{3,i}|^2)/N_s^2 \right) - A_{\text{dB}},$$

where A_{dB} and N_s are constants given by the manufacturer [9, 16]. We use the average FPP during a TWR exchange between t and a, defined as $\mathcal{P}_a := (\mathcal{P}(\hat{R}_{a,1}) + \mathcal{P}(\hat{R}_{t,2}))/2$, in order to build the following model for the measurement variance r

$$r(\mathcal{P}_a; \boldsymbol{\xi}) = \max \left(\sigma^2_{\text{min}}, \alpha 10^{-\beta(\mathcal{P}_a - \mathcal{P}_{\text{max}})} \right) \qquad (1)$$

where $\boldsymbol{\xi} := [\alpha, \beta, \sigma^2_{\text{min}}]$ is a parameter vector to identify. Namely, (1) models the variance of the ranging measurements when the FPP is weaker than a given saturation value

σ^2_{min}, thanks to the second term. Indeed, the parameter σ^2_{min} saturates the value of the variance when the power is sufficient to perform accurate detection.

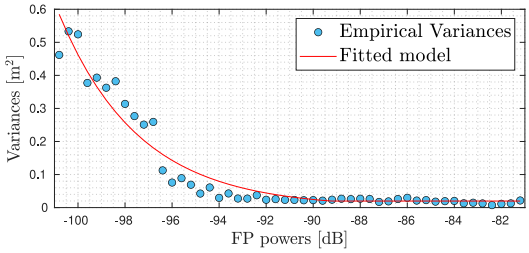

Fig. 3: Empirical variance and model fitting.

To set the model parameters, a robot performs a calibration trajectory among obstacles in a test zone equipped with an MCS and 4 UWB anchors. In Fig. 3 we plot an histogram $\mathcal{H}$ of empirical variance estimates, based on 70000 range and FPP measurements. In our experiment, we grouped these points by power in 50 bins b between $\mathcal{P}_{\text{min}} = -101$ dB and $\mathcal{P}_{\text{max}} = -81$ dB. For each bin b, we compute the empirical variance $\hat{\sigma}_b$ of the range measurements $\tilde{d}_{a,i}$ with FPP falling in that bin, and denote $\mathcal{P}_b$ the central FPP value for the bin. We then set the parameter $\boldsymbol{\xi}$ by solving the following Least-Squares (LS) problem

$$\boldsymbol{\xi} = \underset{\check{\boldsymbol{\xi}}}{\text{argmin}} \sum_{b \in \mathcal{H}} |\hat{\sigma}_b - r(\mathcal{P}_b; \check{\boldsymbol{\xi}})|^2. \tag{2}$$

that can be solved using Levenberg-Marquardt algorithm [17] for instance. The final model is shown on Fig 3.

3.2. Robust Kalman Filter Design

In addition to the variance weighing presented in (1), we use a M-RKF to improve the mitigation of MP outliers. This type of filter uses an M-Estimator to replace the EKF update step. This allows the use of other loss functions than the usual ℓ_2-norm, in order to reduce the influence of large residuals in the estimation process. Since the ranging measurements are contaminated by MP outliers, their distribution is no longer Gaussian and the ℓ_2-norm should be replaced by a more adequate loss function.

Here, we assume that $\tilde{d}_a$ follows an ϵ-contaminated Gaussian observation model, which is a basic model for MP outliers [6]. For this kind of distribution, the *Huber Loss Function* ρ [18], a hybrid between ℓ_1 (efficiently rejecting outliers) and ℓ_2 norms, can be used for the residual $e \in \mathbb{R}$

$$\rho(e) = \begin{cases} c|e| - c^2/2 \text{ if } e^2 > c^2, \\ e^2/2, \text{otherwise.} \end{cases}$$

The parameter c allows us to tune the ℓ_1/ℓ_2 boundary in ρ. In this paper, we set it to 1.345, which ensures a 95% asymptotic relative efficiency for a Gaussian distributed residual e with unitary variance [6, p. 50]. A more detailed discussion on the tuning of c is given in [19].

3.2.1. *Prediction step*

Since we only have access to UWB measurements, we assume a simple linear kinematic model. We define the state vector as $\mathbf{x} = [\mathbf{p}, \dot{\mathbf{p}}]^\top \in \mathbb{R}^{2n}$ and we assume that $\ddot{\mathbf{p}} = \mathbf{w} = [\dots w_i \dots]^\top \in \mathbb{R}^n$, where w_i are independent white Gaussian noises with the same power spectral density S_w. We obtain the discrete state prediction $\mathbf{x}_{k|k-1}$ at time t_k as follows

$$\hat{\mathbf{x}}_{k|k-1} = \mathbf{A}_k \hat{\mathbf{x}}_{k-1|k-1}, \text{ with } \mathbf{A}_k = (\mathbf{I}_{2n} + \mathbf{S}_n \otimes \mathbf{I}_2) h_k, \tag{3}$$

where $h_k = t_k - t_{k-1}$. We denote $\otimes$ the Kronecker product and $\mathbf{S}_n$ the $n \times n$ shift matrix with all its coefficients being zero except $S_{1,n} = 1$. The discrete time version of the process noise is given by a Gaussian random vector $\boldsymbol{\omega}_k \in \mathbb{R}^{2n}$ such that $\boldsymbol{\omega}_k \sim \mathcal{N}(\mathbf{0}, \mathbf{W}_k)$ with $\mathbf{W}_k = S_w \mathbf{G}_k \otimes \mathbf{I}_n$, where $\mathbf{G}_k \in \mathbb{R}^{2\times 2}$ with $G_{k,11} = h_k^3/3$, $G_{k,12} = G_{k,21} = h_k^2/2$, $G_{k,22} = h_k$. Then, the prediction's covariance is given by

$$\mathbf{P}_{k|k-1} = \mathbf{A}_k \mathbf{P}_{k-1|k-1} \mathbf{A}_k^\top + \mathbf{W}_k. \tag{4}$$

3.2.2. *M-RKF Update*

Then, we incorporate the distance measurement $\tilde{d}_a$ from anchor a, considering that $\tilde{d}_a \sim \mathcal{N}(d_a, r(\mathcal{P}_a))$, where $r(\mathcal{P}_a)$ is set using (1) and the FPP measurement. Define the Jacobian matrix $\mathbf{J}_{a,k} = \partial d_a / \partial \mathbf{x}|_{\mathbf{x}_{k|k-1}} = [(\hat{\mathbf{p}}_{k|k-1} - \mathbf{p}_a)^\top / \hat{d}_a, \mathbf{0}_{1,n}]$ of d_a with respect to the state, where $\hat{d}_a := \|\hat{\mathbf{p}}_{k|k-1} - \mathbf{p}_a\|$. Then, we follow the M-RKF update as defined in [6, Section 7.4]. First, we define the augmented state equation

$$\mathbf{z}_k = \mathbf{H}_k \mathbf{x}_k + \boldsymbol{\mu}_k \tag{5}$$

where $\mathbf{z}_k = [\hat{\mathbf{x}}_{k|k-1}^\top, \tilde{d}_a - \hat{d}_a + \mathbf{J}_{a,k} \hat{\mathbf{x}}_{k|k-1}]^\top$ and $\mathbf{H}_k = [\mathbf{I}_{2n}, \mathbf{J}_a^\top]^\top$. The covariance of $\boldsymbol{\mu}_k$ can be written as the diagonal block matrix $\check{\mathbf{P}}_k := \mathbb{E}\{\boldsymbol{\mu}_k \boldsymbol{\mu}_k^\top\} = \text{diag}(\mathbf{P}_{k|k-1}, r_a)$.

Now, we need to normalize the noise variances on $\mathbf{z}_k$ in order to apply the M-estimation step. Since $\check{\mathbf{P}}_k$ is a positive definite matrix, it admits a square root $\mathbf{Q}_k$ such that $\check{\mathbf{P}}_k = \mathbf{Q}_k \mathbf{Q}_k^\top$, which can be obtained by Cholesky factorization [20]. Then, we normalize the noise variances in (5) by left-multiplying it by $\mathbf{Q}_k^{-1}$, so that $\bar{\boldsymbol{\mu}}_k = \mathbf{Q}_k^{-1} \boldsymbol{\mu}_k$ satisfies $\mathbb{E}\{\bar{\boldsymbol{\mu}}_k \bar{\boldsymbol{\mu}}_k^\top\} = \mathbf{I}_{2n+1}$.

Then, we solve the following M-estimation problem

$$\mathbf{x}_{k|k} = \underset{\mathbf{x} \in \mathbb{R}^{2n}}{\text{argmin}} \sum_{i=1}^{2n+1} \rho(e_i(\mathbf{x})), \tag{6}$$

where $e_i(k)$ denotes the i-th component of the residual vector $\mathbf{e}(\mathbf{x}) := \mathbf{Q}_k^{-1}(\mathbf{z}_k - \mathbf{H}_k \mathbf{x})$. In practice, the problem (6) can be solved using the following iterations [6, Section 2.5]

$$\begin{cases} \boldsymbol{\Omega}^l = \text{diag}(\dots \omega(e_i(\mathbf{x})) \dots), \\ \mathbf{x}^{l+1} = (\bar{\mathbf{H}}_k^\top \boldsymbol{\Omega}^l \bar{\mathbf{H}}_k)^{-1} \bar{\mathbf{H}}_k^\top \boldsymbol{\Omega}^l \mathbf{Q}_k^{-1} \mathbf{z}_k, \end{cases} \quad l \in [1, N] \tag{7}$$

with the weights $\omega(e_i(\mathbf{x})) := \min\{1, c/|e_i(\mathbf{x})|\}$, where $\bar{\mathbf{H}}_k = \mathbf{Q}_k^{-1} \mathbf{H}_k$ and setting $\mathbf{x}^0 = \hat{\mathbf{x}}_{k|k-1}$ as initial condition. We define the stopping condition of the iterations

(7) as $\|\mathbf{x}^N - \mathbf{x}^{N-1}\|/\|\mathbf{x}^{N-1}\| < \delta$ at the iteration N, where $\delta > 0$ defines a tolerance threshold. We then set $\hat{\mathbf{x}}_{k|k} := \mathbf{x}^N$ and the prediction covariance can be approximated by $\mathbf{P}_{k|k} \approx (\bar{\mathbf{H}}_k^\top \boldsymbol{\Omega}^N \bar{\mathbf{H}}_k)^{-1}$.

Note that the standard EKF algorithm is obtained replacing ρ by the ℓ_2-norm, *i.e.*, when the parameter $c \to \infty$; or equivalently, by setting the weights $\boldsymbol{\Omega}^i$ uniformly to $\mathbf{I}_{2n+1}$.

4. EXPERIMENTS

We present two localization experiments involving the setup shown in Fig. 2. The robot acquires UWB measurements with a transceiver that ranges with four anchors at a refresh rate of about 280 Hz. The range measurements are obtained using the TWR protocol presented in [15]. The first experiments is performed with obstacles present in the testing area (*strong scenario*), the second without (*mild scenario*). The anchor locations, the obstacles and the trajectories are plotted in Fig. 4 for both scenarios. After acquiring both UWB and reference MCS data, we post-processed them to test the methodology presented in the previous section.

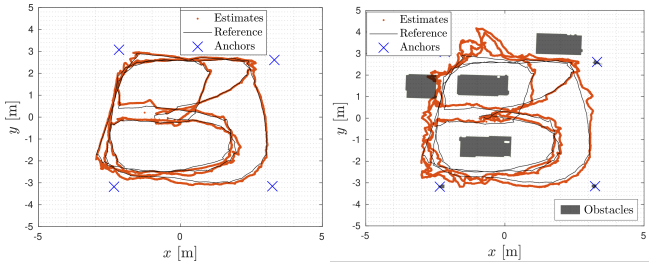

(a) Mild scenario. (b) Strong scenario.

Fig. 4: Trajectories and estimates (M-RKF output).

For both experiments we implemented a standard EKF, a standalone M-RKF, as well as both filters using variances computed by the FPP model (1) (denoted EKF+FPP and M-RKF+RPP respectively). For both (M-RKF) and (EKF), we choose a constant measurement noise variance $r = (0.2)^2$ m^2. For the implementations using the FPP-based variance model, we set $\alpha = 2.1 \times 10^{-4}$, $\beta = 0.16$ and $\sigma_{\text{min}} = (0.14)^2$ m^2, after calibration trajectory using (2). We set the process noise spectral density to $\sigma_w^2 = (0.14)^2$ m^2/s^3.

Table 1: Empirical RMSE comparison.

Test/Filter	EKF	EKF/FPP	M-RKF	M-RKF+FPP
Mild [cm]	20.5	18.4	17.7	16.3
Strong [cm]	43.6	38.1	30.1	29.6

We show in Table 1 the empirical Root Mean Square Error (RMSE) computed from the trajectories (we skipped the points where the robot was static) for the two scenarios and all the EKF/M-RKF implementations. Compared to the performance of the EKF, for both scenarios we can notice a significant improvement (10% *mild*, 13% *strong*) from using the calibrated FPP-based variance model $r(\mathcal{P}_a)$. The M-RKF, even without the power correction, provides a much improved localization performance (14% *mild*, 31% *strong*). This is not surprising since it was tailored to mitigate data contamination. Finally, the complete M-RKF framework with FPP-based variance $r(\mathcal{P}_a)$ yields a 20% RMSE reduction for the *mild* scenario and a 32% improvement for the *strong* scenario.

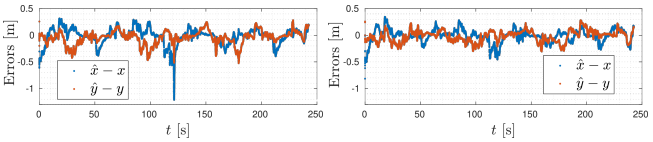

(a) EKF. (b) M-RKF+FPP.

Fig. 5: Positioning error plots for the *mild* scenario.

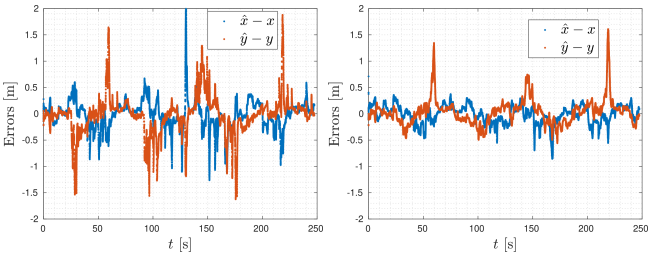

(a) EKF. (b) M-RKF+FPP.

Fig. 6: Positioning error plots for the *strong* scenario.

These results are further illustrated in Figs. 5 and 6 by plotting the components of the errors $\hat{\mathbf{p}} - \mathbf{p}$ over time. We remark that the localization performance for the *mild* scenario is fair while using the M-RKF+FPP algorithm. The computational time is also reasonable, as we allowed a maximum of 10 iterations in (7). However, the *strong* scenario highlights difficulties when the robot's heading is changing. Indeed, our prediction model (3) is simplistic and does not include heading observations. Hence, to reach suitable navigation performance when the measurements are strongly deteriorated, we suggest to refine the robot's dynamic model. Moreover, additional anchors can be added in order to provide line-of-sight measurements to the robot, in particular in the top left zone as shown in Fig. 4b.

5. CONCLUSION AND PERSPECTIVES

In this paper, we first proposed calibrating an empirical variance model for UWB range measurements deduced from ToF estimates, based on the received FPP. Then, we designed a robust M-RKF to design an UWB-based navigation system in the presence of MP outliers. Finally, we validated through experiments the benefits of both our variance model and the M-RKF, with real-world data contaminated by MP. Future work will include odometry and inertial coupling to make the solution fully operational for robot navigation in challenging environments.

6. REFERENCES

[1] Amanda Prorok, *Models and Algorithms for Ultra-Wideband Localization in Single- and Multi-Robot Systems*, Ph.D. thesis, École Polytechnique Fédérale de Lausanne, Lausanne, 2013.

[2] Zafer Sahinoglu, Sinan Gezici, and Ismail Guvenc, *Ultra-wideband Positioning Systems: Theoretical Limits, Ranging Algorithms, and Protocols*, Cambridge University Press, Cambridge, cambridge university press edition, 2008.

[3] Bernhard Etzlinger and Henk Wymeersch, "Synchronization and Localization in Wireless Networks," *Foundations and Trends® in Signal Processing*, vol. 12, pp. 1–106, Jan. 2018.

[4] Paul D. Groves, *Principles of GNSS, inertial, and multisensor integrated navigation systems*, Artech House, 2nd edition, 2013.

[5] Changhui Jiang, Jichun Shen, Shuai Chen, Yuwei Chen, Di Liu, and Yuming Bo, "UWB NLOS/LOS Classification Using Deep Learning Method," *IEEE Communications Letters*, vol. 24, no. 10, pp. 2226–2230, Oct. 2020.

[6] Abdelhak M. Zoubir, Visa Koivunen, Esa Ollila, and Michael Muma, *Robust Statistics for Signal Processing*, Cambridge University Press, 1 edition, 2018.

[7] Zhuoqi Zeng, Steven Liu, and Lei Wang, "NLOS Detection and Mitigation for UWB/IMU Fusion System Based on EKF and CIR," in *2018 IEEE 18th International Conference on Communication Technology (ICCT)*, Oct. 2018, pp. 376–381, ISSN: 2576-7828.

[8] K. Bregar and M. Mohorčič, "Improving Indoor Localization Using Convolutional Neural Networks on Computationally Restricted Devices," *IEEE Access*, vol. 6, pp. 17429–17441, 2018.

[9] Karthikeyan Gururaj, Anojh Kumaran Rajendra, Yang Song, Choi Look Law, and Guofa Cai, "Real-time identification of NLOS range measurements for enhanced UWB localization," in *2017 International Conference on Indoor Positioning and Indoor Navigation (IPIN)*, Sept. 2017, pp. 1–7, ISSN: 2471-917X.

[10] Xu-hong Li and Tongli Zhang, "Research on Improved UWB Localization Algorithm in NLOS Environment," in *2018 International Conference on Intelligent Transportation, Big Data & Smart City (ICITBS)*, Jan. 2018, pp. 707–711.

[11] Qichao Zhu, Chao Yu, Henghao Gu, and Zuokun Li, "Application Research of UWB Indoor Reverse Positioning Based on Robust Kalman Filtering," in *2020 IEEE 20th International Conference on Communication Technology (ICCT)*, Oct. 2020, pp. 571–577, ISSN: 2576-7828.

[12] Wenda Zhao, Jacopo Panerati, and Angela P. Schoellig, "Learning-Based Bias Correction for Time Difference of Arrival Ultra-Wideband Localization of Resource-Constrained Mobile Robots," *IEEE Robotics and Automation Letters*, vol. 6, no. 2, pp. 3639–3646, Apr. 2021, Conference Name: IEEE Robotics and Automation Letters.

[13] Xin Li, Yan Wang, and Kourosh Khoshelham, "UWB/PDR Tightly Coupled Navigation with Robust Extended Kalman Filter for NLOS Environments," *Mobile Information Systems*, vol. 2018, pp. e8019581, Dec. 2018, Publisher: Hindawi.

[14] Yi Ding, Paul Chauchat, Gaël Pages, and Philippe Asseman, "Learning-Enhanced Adaptive Robust GNSS Navigation in Challenging Environments," *IEEE Robotics and Automation Letters*, vol. 7, no. 4, pp. 9905–9912, Oct. 2022.

[15] Justin Cano, Gael Pages, Eric Chaumette, and Jerome Le Ny, "Clock and Power-Induced Bias Correction for UWB Time-of-Flight Measurements," *IEEE Robotics and Automation Letters*, pp. 1–1, 2022.

[16] Qorvo (formerly Decawave), *DWM1000 datasheet*, 2022, `https://www.qorvo.com/products/p/DWM1000`.

[17] Henri P Gavin, "The Levenberg-Marquardt algorithm for nonlinear least squares curve-fitting problems," Tech. Rep., Department of Civil and Environmental Engineering, Duke University, 2019.

[18] Peter J. Huber, "Robust Estimation of a Location Parameter," *The Annals of Mathematical Statistics*, vol. 35, no. 1, pp. 73–101, Mar. 1964.

[19] Lili Wang, Chao Zheng, Wen Zhou, and Wen-Xin Zhou, "A new principle for tuning-free huber regression," *Statistica Sinica*, 2020.

[20] Kaare Brandt Petersen and Michael Syskind Pedersen, "The Matrix Cookbook," Tech. Rep., Technical University of Denmark, 2012.